Photodissociation of N_2O. I. Ab Initio Potential Energy Surfaces for the Low-Lying Electronic States $\tilde{X}\ ^1A'$, $2\ ^1A'$, and $1\ ^1A''$

Alex Brown, Pedro Jimeno, and Gabriel G. Balint-Kurti*

School of Chemistry, The University of Bristol, Bristol, BS8 1TS, U.K.

Received: June 24, 1999; In Final Form: September 20, 1999

Adiabatic potential energy surfaces of the three lowest lying singlet states, $\tilde{X}\ ^1A'$ $2\ ^1A'$, and $1\ ^1A''$, of N_2O have been computed as a function of the R_{N_2-O} bond distance and the Jacobi angle. The calculations are performed using the complete-active-space self-consistent field (CASSCF) and the multireference configuration interaction (MRCI) electronic structure methods. It is shown that there is a wide avoided crossing between the ground, $\tilde{X}\ ^1A'$, and lowest excited, $2\ ^1A'$, electronic state. This avoided crossing is thought to give rise to a seam of conical intersection at other N−N separations. Both excited state surfaces display important conical intersections at linear geometries. The transition dipole moment surfaces for the two excitation processes ($2\ ^1A' \leftarrow \tilde{X}\ ^1A'$ and $1\ ^1A'' \leftarrow \tilde{X}\ ^1A'$) are also presented. These calculations provide the basic data needed to compute the dynamics of the $N_2O + h\nu \rightarrow N_2 + O(^1D)$ photodissociation process for photon frequencies in the range 5.2 eV (240 nm) to 7.3 eV (170 nm).

1. Introduction

The nitrous oxide molecule plays an important role in both atmospheric and combustion chemistry. The photodissociation process

$$N_2O + h\nu \rightarrow N_2(\tilde{X}\ ^1\Sigma_g^+) + O(^1D) \qquad (1)$$

which produces nitrogen in its ground electronic state, $N_2(\tilde{X}\ ^1\Sigma_g^+)$, and electronically excited state oxygen $O(^1D)$, is of particular interest.

The above reaction is important both atmospherically and in combustion because it is a source of highly reactive oxygen atoms in their first excited electronic state. Of more practical application, the photodissociation of N_2O is often used in the laboratory as a source of $O(^1D)$ atoms for reaction dynamics and kinetics experiments.[1−3] The main benefits of using the photodissociation process as a source of $O(^1D)$ are that it comprises the major oxygen dissociation channel and that the other partner in the photodissociation process, N_2, is chemically inert.

The photodissociation of N_2O has received a great deal of experimental interest.[4−10] The ultraviolet absorption spectrum of N_2O is a very broad peak with superimposed diffuse structure which runs from about 5.2 to 7.3 eV (170 to 240 nm) and with a maximum near 6.9 eV (180 nm).[11] More detailed dynamics experiments have been carried out in the long-wavelength tail, 6.4 or 6.1 eV (193 or 205 nm), to measure the energetics and spatial distributions of the photofragments. The experiments have shown that the N_2 produced is highly rotationally excited, mainly vibrationally cold, and that the average anisotropy parameter, β, is approximately 0.5. Recent experiments[4−6] have shown that there are added complexities involved in the photodissociation dynamics. Neyer et al.[4] have determined the J-dependent spatial anisotropy for the N_2 fragment. They have shown that while β is positive for all rotational states ($J = 40-90$), the anisotropy decreases for increasing rotational state. The correlations between the speed and angular distributions of the $O(^1D)$ fragment have been measured by Suzuki et al.[6] Their results indicate that there are multiple paths to dissociation and point to the fact that there may be orbital alignment of the $O(^1D)$ products. From the experimental studies, it is obvious that the photodissociation of N_2O represents a very rich dynamical process.

Despite the experimental interest in N_2O, there has been little recent theoretical study of this system[12−19] focusing on the dissociation process of eq 1; most theoretical studies[20,21] have examined the spin-forbidden process involving the quenching of $O(^1D)$ to $O(^3P)$ by collisions with N_2. The most recent ab initio study of N_2O by Hopper[12] provides an excellent overview of the low-lying excited state potential energy surfaces. However, no transition dipole moments have been computed and the calculations were performed at an insufficient number of nuclear geometries to permit subsequent dynamical calculations. It is now possible to compute more accurate potential energy surfaces than those reported by Hopper[15] years ago and to provide a fuller sampling of the nuclear geometries needed to perform the subsequent dynamics.

In the current article, we present new potential energy surfaces, and the transition dipole moment surfaces between them, for the three lowest singlet states of N_2O, $\tilde{X}\ ^1A'$ $2\ ^1A'$, and $1\ ^1A''$. Section 2 provides a description of the ab initio methods used for the calculations. The potential energy surfaces and the transition dipole moment surfaces, and their implications for the photodissociation dynamics of N_2O, are discussed in section 3. A full time-dependent wavepacket treatment of the N_2O photodissociation dynamics will be presented in a forthcoming paper. The conclusions of the work are given in section 4.

2. Computational Methods

The calculations described in this paper were performed using the MOLPRO ab initio molecular electronic structure program.[22]

* To whom correspondence should be addressed. E-mail: Gabriel.Balint-Kurti@bristol.ac.uk.

10.1021/jp992116r CCC: $18.00
Published on Web 11/24/1999

We have used the state-averaged complete active space self-consistent field (CASSCF)[23,24] and multireference configuration interaction (MRCI)[25,26] methods. State-averaged calculations are necessary in order to obtain a common set of orbitals which can subsequently be used for the transition dipole moment calculations. The state-averaging procedure also has the advantage that the different electronic states are treated in a balanced manner. The calculations were performed over a grid of nuclear geometries. Once the grid of ab initio points had been obtained, the potential energy surfaces were interpolated using the reproducing kernel Hilbert space method,[27,28] while the transition dipole moment surfaces were interpolated using a spline fitting procedure.

The calculations have been performed using the augmented correlation consistent valence double zeta (avdz) basis set of Dunning.[29,30] This basis consists of the correlation consistent valence double zeta basis of Dunning augmented by (1s1p) diffuse functions and by 1d polarization function. Previous calculations on N_2O by Hopper[12] utilized the double zeta plus polarization (DZP) basis of Dunning.[31] Theoretical investigations of similar species, e.g. O_3,[32−35] and OCS,[37] have shown that a DZP basis set gives a reliable description of the lowest potential energy surfaces and the shapes of the transition dipole moment surfaces. The present study is the first to compute the transition dipole moments, $2\ ^1A' \leftarrow \tilde{X}\ ^1A'$ and $1\ ^1A'' \leftarrow X\ ^1A'$. The shapes of the transition dipole moment surfaces and their relative values will be of particular interest in connection with the photodissociation process.

The full-valence active space would comprise all 2s and 2p orbitals. This active space involves 17 electrons distributed around 12 active orbitals. Alternatively, as has been used in calculations for ozone[32,33,36] and OCS,[37] an active space comprising only the 2p valence orbitals can be utilized. The number of configuration state functions (CSF's) for these two active spaces are 35 793 for A′ symmetry and 34 992 for A″ symmetry for the full-valence active space, while for the reduced active space, the number of CSF's is 2688 and 2604 for A′ and A″ symmetries, respectively. We present CASSCF results for both active spaces and conclude that the inclusion of the 2s orbitals is not needed. Therefore, subsequent MRCI calculations only utilize CASSCF orbitals calculated using the smaller active space. It was not computationally feasible to include all configurations during the MRCI calculations, so only excitations from the main contributing CSF's at the CASSCF level (contribution greater than 0.05) were included which reduced the number of configurations to around 600 000.

The ground state of N_2O is linear and belongs to the $C_{\infty v}$ point group. The molecular orbitals and the electronic configuration of the ground state valence orbitals can be described as $(4\sigma)^2(5\sigma)^2(6\sigma)^2(1\pi)^4(7\sigma)^2(2\pi)^4(3\pi)^0(8\sigma)^0(9\sigma)^0$ in the notation of this point group. However, all electronic structure calculations were performed using the C_s symmetry group which is the appropriate group for bent geometries. In C_s symmetry, the molecular orbitals and the electron occupancies of the ground state can be described as $(4a')^2(5a')^2(6a')^2(7a')^2(1a'')^2(8a')^2$-$(2a'')^2(9a')^2(10a')^0(3a'')^0(11a')^0(12a')^0$. These orbitals will be useful for the description of the major contributions to the various states. In the linear configuration, i.e. $C_{\infty v}$ symmetry, the ground state has $^1\Sigma^+$ symmetry. It correlates in a bent nuclear geometry with a state of $^1A'$ symmetry (the $\tilde{X}\ ^1A'$ state). The lowest excited state, $1\ ^1A''$, correlates in linear geometries with a state of $^1\Sigma^-$ symmetry at bond lengths within the Franck−Condon region while correlating with a $^1\Pi$ state for long N−O bond lengths. Finally, the $2\ ^1A'$ state (second excited state) is associated with a $^1\Delta$ state for bond lengths within the Franck−Condon region while correlating with a $^1\Pi$ state asymptotically and at very short bond lengths (less than 3.1 bohr). These assignments will become more clear in the discussion of the potential energy surfaces and transition dipole moments in the following section.

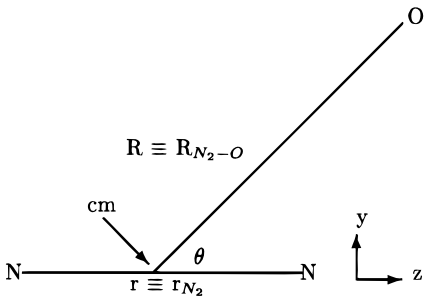

Figure 1. Definition of the Jacobi coordinate system used in the present work. Also shown are the directions of the *y*- and *z*-axes used in defining the transition dipole moment.

TABLE 1: Bond Dissociation Energies for N_2O for Various Methods

method	D_e (eV)
CASSCF1[a,b]	2.014
CASSCF2[a,c]	2.578
MR-CI[a,d]	3.487
Hopper[e]	3.12
experimental D_o[f]	3.639
experimental D_e[g]	3.785

[a] The bond dissociation energies are defined relative to the following (unoptimized) geometries: $\tilde{X}\ ^1A'$ minimum $(R,r,\theta) = (3.3,2.131\ 99,180)$, asymptote (1000,2.131 99,180). [b] State-averaged CASSCF with 2p orbitals active. Two A′ and one A″ states were averaged with equal weights. [c] State-averaged CASSCF with 2s and 2p orbitals active. Two A′ and one A″ states were averaged with equal weights. [d] Internally contracted MRCI with CASSCF1 as reference. Includes Davidson correction. [e] MCSCF/CI using double zeta plus d-polarization functions at the geometry $(R,r,\theta) = (3.303\ 805,\ 2.131\ 99,0)$ from ref 12. [f] Reference 40. [g] Obtained after correcting for the zero-point energies using the harmonic approximation and frequencies from ref 41.

3. Results and Discussion

3.1. Potential Energy Surfaces. The three lowest singlet potential energy surfaces of N_2O were computed using the MRCI method together with the Davidson correction[39] for size consistency. We have used the Jacobi coordinate system in the present work. Figure 1 shows the chosen coordinate system; note that the molecule is linear for $\theta = 0°$ and that θ is restricted to values $0 \le \theta \le \pi/2$. In all the calculations, the N_2 bond distance was held fixed at the experimental value in N_2O of 2.131 99 bohr. This is justified by the fact that the N_2 bond distance contracts less then 3% (from 2.131 99 bohr in N_2O to 2.074 16 bohr in N_2) during the photodissociation process. Hence, no significant contribution is expected from the stretching of the N−N bond. Accordingly, the photodissociation of N_2O produces vibrationally cold N_2;[7] the amount of $v = 1$ is less than 2% of the $v = 0$ product.

Our computed bond dissociation energies at a variety of levels of theory are given in Table 1 and compared with previous calculations and with the experimental results. Note that the geometry of N_2O has not been optimized in the present calculations as the main goal is to produce reliable potential energy surfaces over a wide range of geometries. However, it is worth comparing the bond dissociation energy as defined from

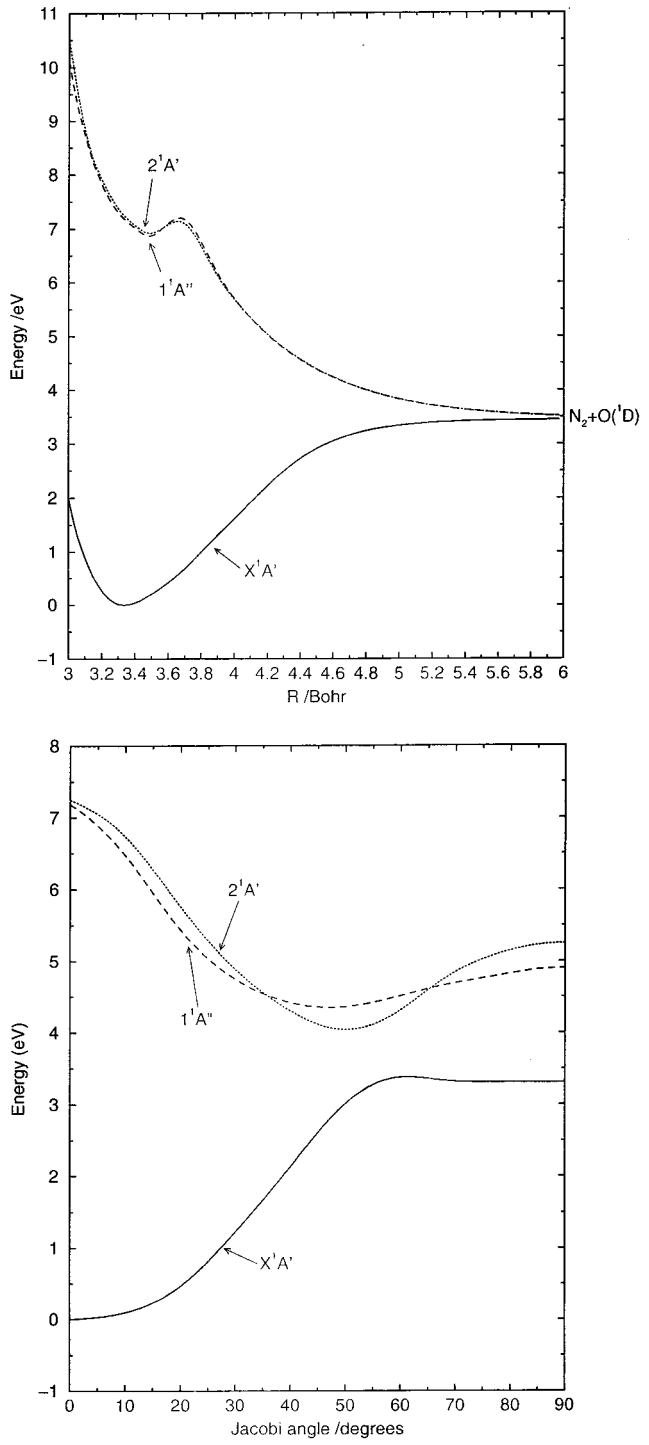

Figure 2. Cuts through the three lowest singlet state potentials: (A, top) variation of the potentials with Jacobi coordinate R in the N−N−O collinear geometry; (B, bottom) variation of the potentials with Jacobi angle and with the N_2−O separation fixed at the ground state equilibrium value (3.334 bohr). All energies are defined relative to the minimum energy at the ground state equilibrium separation.

the minimum in the potential energy surface, $(R,r,\theta) = (3.3,2.13199,0)$, with previous results in order to extract a measure of the reliability of the present calculations. Neither of the CASSCF calculations provides a reliable estimate of the bond dissociation energy. However, once the nondynamical correlation is included via the MRCI ansatz, we obtain a dissociation energy, 3.487 eV, which is within 8% of the experimental dissociation energy of 3.785 eV. On the basis of this good agreement, we have decided that omitting the 2s orbitals from the active space is an adequate approximation for the present study.

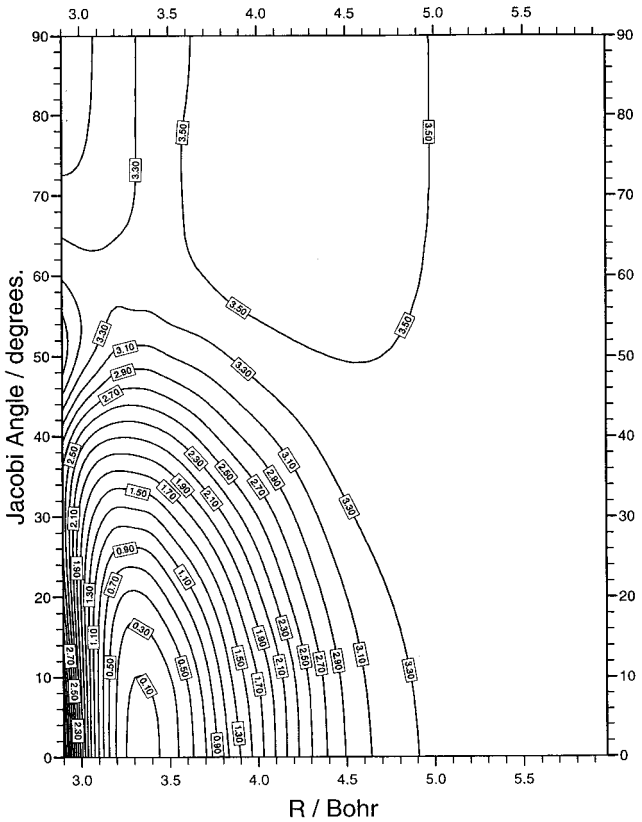

Figure 3. Contour plot of the adiabatic potential energy surface for the $\tilde{X}\ ^1A'$ ground electronic state of N_2O as a function of Jacobi coordinates R and θ with $r_{N_2} = 2.131\,99$ bohr. The lowest energy contour is a 0.1 eV above the computed minimum of the surface and the contours are spaced at 0.2 eV intervals. The depth of the well in the surface is 3.487 eV.

Figure 2 presents two cuts through the three lowest singlet surfaces. In Figure 2A, the Jacobi angle is held fixed at 0°, i.e., linear, and the N_2−O bond distance is varied. The figure shows that all three surfaces dissociate adiabatically to yield $N_2(\tilde{X}\ ^1\Sigma_g^+)$ and $O(^1D)$. Figure 1B shows the variation of the three lowest singlet surfaces as a function of the Jacobi angle θ and with the N_2−O separation held fixed at its equilibrium value in the ground state ($R = 3.334$ bohr). An avoided crossing between the two lowest $^1A'$ states is clearly seen to be present. This avoided crossing is discussed further below, and we speculate that in other geometries it becomes a seam of conical intersection.

The contour diagram of the potential energy surface for the ground, $\tilde{X}\ ^1A'$, electronic state is shown in Figure 3. The figure is based on the computation of the energy at 130 different geometries over a grid representing 13 different bond lengths for R_{N_2-O} (from 2.9 to 6.0 bohr) and 10 different Jacobi angles with a 10° spacing. These points are then interpolated using the reproducing kernel Hilbert space method[27,28] to give the contour plot illustrated. The ground state geometry is linear as seen by the deep well, depth 3.487 eV, for the Jacobi angle of 0°. There is a ridge in the potential surface running between $(R_{N_2-O},\theta) = (2.9,50°)$ and (3.5,60°). This feature is due to the interaction with the low-lying 2 $^1A'$ state. It will be discussed below and is being further investigated. Note that a cut through the potential taken at a Jacobi angle of 90° would show a maximum at long range ($R \approx 4.3$ bohr) and a minimum at a smaller value of the Jacobi scattering coordinate ($R \approx 2.9$ bohr).

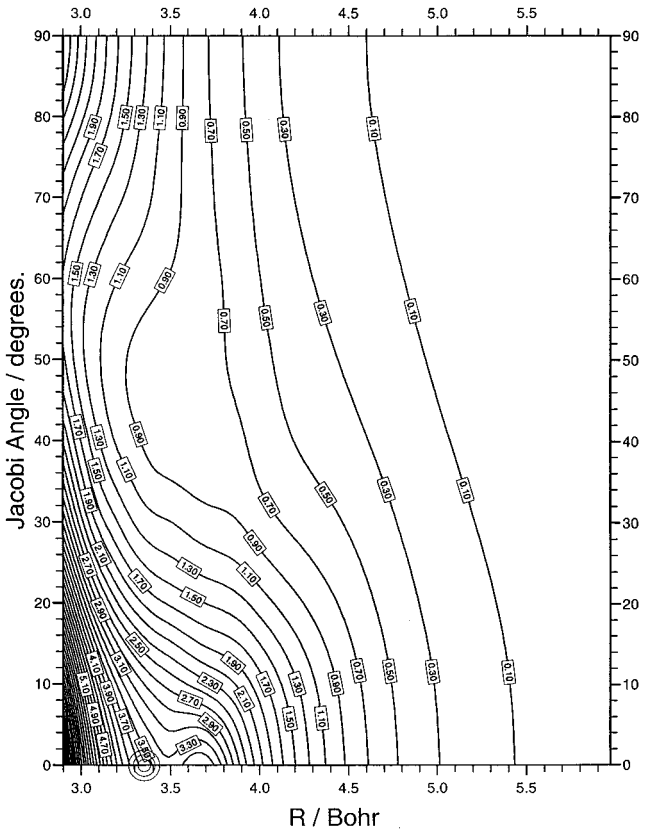

Figure 4. Contour plot of the adiabatic potential energy surface for the 1 ^{1}A″ excited electronic state of N_2O as a function of Jacobi coordinates R and θ with r_{N_2} = 2.131 99 bohr. The lowest energy contour is at 0.1 eV above the asymptotic energy and the contours are spaced at 0.2 eV intervals.

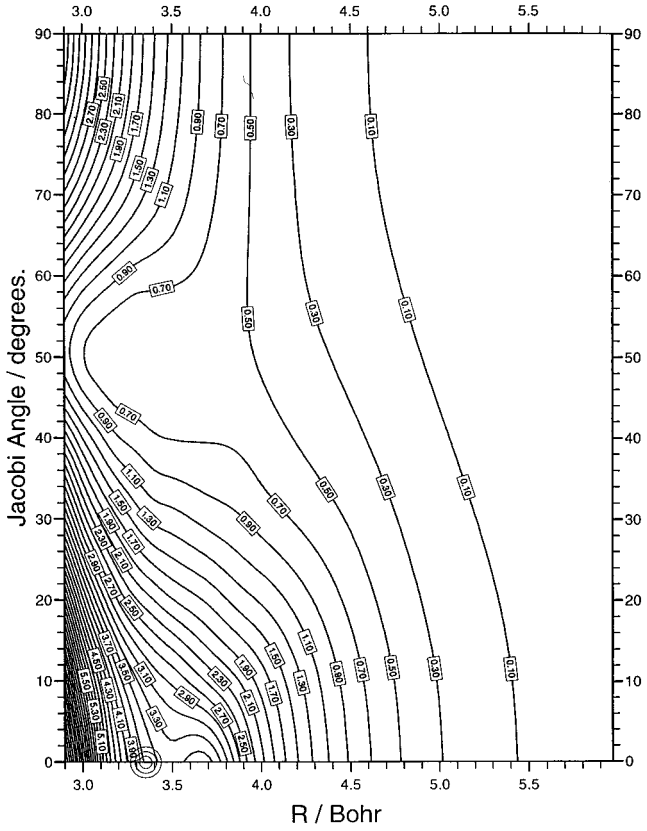

Figure 5. Contour plot of the adiabatic potential energy surface for the 2 ^{1}A′ excited electronic state of N_2O as a function of Jacobi coordinates R and θ with r_{N_2} = 2.131 99 bohr. The lowest energy contour is at 0.1 eV above the asymptotic energy and the contours are spaced at 0.2 eV intervals.

The contour diagrams of the two excited singlet states, 1 ^{1}A″ and 2 ^{1}A′, are illustrated in Figure 4 and 5, respectively, and have been obtained by the same methods as were used for the ground state surface. A minimum energy seam on the 2 ^{1}A′ surface which corresponds with the $\tilde{X}$ ^{1}A′ maximum seam is clearly visible in Figure 5. Both excited state surfaces have a maximum near 3.65 bohr for linear geometries. For the 1 ^{1}A″ state this represents a conical intersection between the $^1\Sigma^-$ state and the A″ component of the $^1\Pi$ state. On the other hand, the linear maximum on the 2 ^{1}A′ surface represents a conical intersection between the $^1\Delta$ state and the A′ component of the $^1\Pi$ state.

The position of the minimum on the ground state surface, i.e., the Franck−Condon geometry, is marked on both of the excited state surface contour plots (Figure 4 and 5). From the contour plots, it is clear that as N_2O dissociates, substantial torque will be imparted to the N_2 fragment resulting in high rotational excitation. This qualitative observation is borne out in the experimental results where the rotational state distributions of the N_2 photofragment peaks near J = 70. The conical intersections on the two excited electronic state surfaces lie close to the Franck−Condon geometries, (R,θ) = (3.35,0°), and will clearly have an important effect on the photodissociation dynamics. Their main effect on the dynamics will be to distort the adiabatic surfaces so as to create a torque in the departing N_2 diatomic fragment.

Figure 6 shows cuts through the $\tilde{X}$ ^{1}A′ and 2 ^{1}A′ potential energy surfaces as a function of Jacobi angle for fixed R_{N_2-O} bond lengths of 3.1, 3.0, and 2.9 bohr near their seam of intersection. The two state approach to within 0.5 eV. While this avoided crossing at bent geometries has been seen before, see Hopper,[12] no extensive examination of this region has been carried out. Preliminary CASSCF calculations with the avdz basis set show that the states can approach to within 0.001 eV (our threshhold for minimum energy difference convergence) for geometries which allow the N−N bond distance to relax. This illustrates that either a non-symmetry-related conical intersection or a very sharp avoided crossing is located in this region of nuclear geometries. Further studies of the region as a function of all three Jacobi variables are currently underway.

TABLE 2: Vertical Excitation Energies for N_2O for Various Methods

method	2 ^{1}A′ T_e (eV)	1 ^{1}A″ T_e (eV)
CASSCF1[a,b]	7.765	7.255
CASSCF2[a,c]	7.684	7.468
MR-CI[a,d]	7.352	7.280
Hopper[e]	7.7	7.6

[a] The vertical excitation energies are defined relative to the following (unoptimized) ground state $\tilde{X}$ ^{1}A′ geometry minimum (R,r,θ) = (3.3,2.131 99,180). [b] State-averaged CASSCF with 2p orbitals active. Two A′ and one A″ states were averaged with equal weights. [c] State-averaged CASSCF with 2s and 2p orbitals active. Two A′ and one A″ states were averaged with equal weights. [d] Internally contracted MRCI with CASSCF1 as reference. Includes Davidson correction. [e] MCSCF/CI using double zeta plus d-polarization plus diffuse functions from ref 12.

The calculated vertical excitation energies along with Hopper's[12] previous results are given in Table 2. The detailed dynamics experiments have been carried out at photon energies of 6.4 or 6.0 eV (193 or 205 nm). From our computed vertical excitation energies of 7.28 and 7.35 eV to the 1 ^{1}A″ and 2 ^{1}A′ states, it seems unlikely that vibrationally cold N_2O, where most

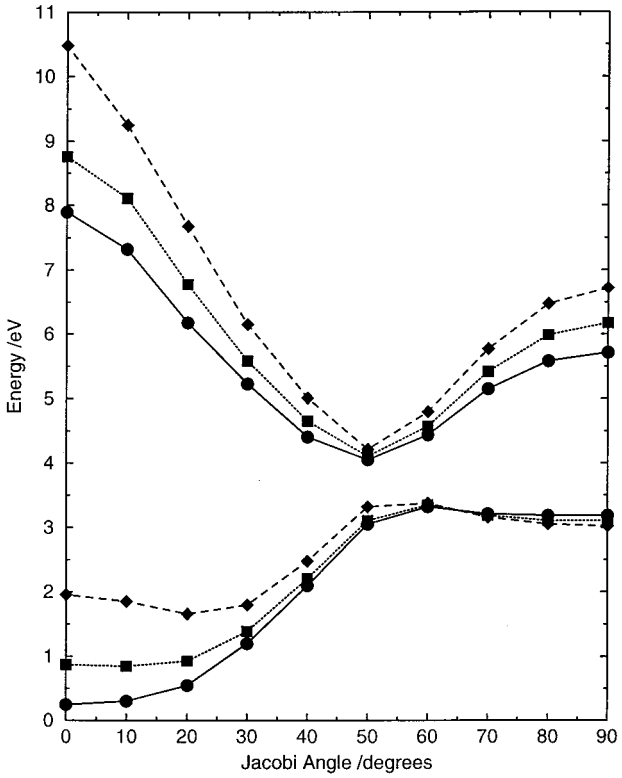

Figure 6. Cuts through the $\tilde{X}\ ^1A'$ and $2\ ^1A'$ potential energy surfaces of N_2O as a function of Jacobi angle with the N_2-O bond distance set equal to 3.1 (●), 3.0 (□), and 2.9 (◇) bohr. The energy is relative to the minimum in the $\tilde{X}\ ^1A'$ state.

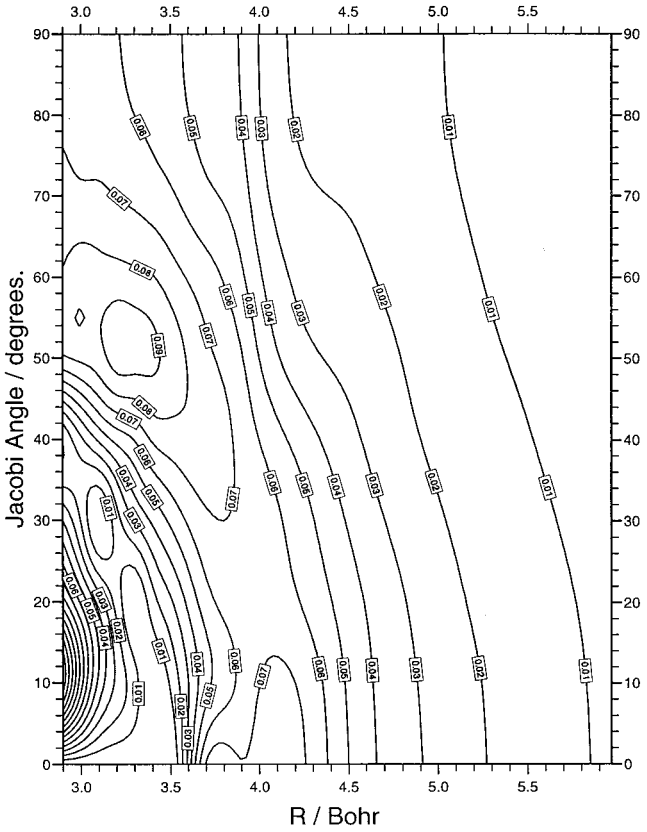

Figure 7. Contour plot of the transition dipole moment surface for the $1\ ^1A'' \leftarrow \tilde{X}\ ^1A'$ transition as a function of Jacobi coordinates R and θ with $r_{N_2} = 2.131\ 99$ bohr. The transition dipole is perpendicular to the molecular plane and is given in atomic units. The value of the lowest contour is 0.01 au and the contour spacing is 0.01 au.

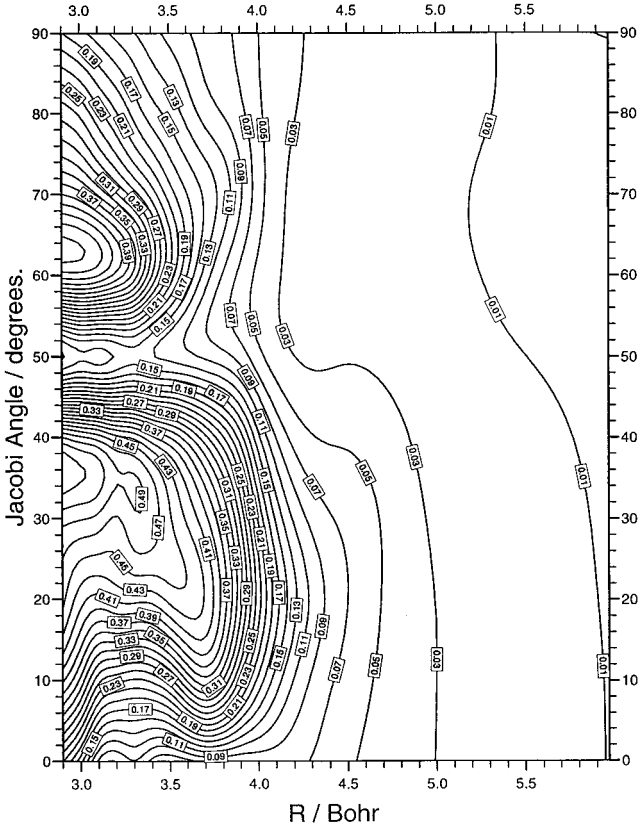

Figure 8. Contour plot of the magnitude of the transition dipole moment for the $2\ ^1A' \leftarrow \tilde{X}\ ^1A'$ transition as a function of Jacobi coordinates R and θ with $r_{N_2} = 2.131\ 99$ bohr. The direction of the transition dipole moment varies but it is always in the molecular plane. The magnitude of the transition moment is given in atomic units. The transition dipole is perpendicular to the molecular plane and is given in atomic units. The value of the lowest contour is 0.01 au and the contour spacing is 0.02 au.

of the wave function resides close to the Franck−Condon region, can be photodissociated with a high probability at these photon energies. This conclusion is also supported by the previous calculations of Hopper.[12] However, even for a modest bending angle of 10° these vertical excitation energies are reduced to 6.7 and 6.5 eV, respectively. Therefore, if the bending mode of the ground state were excited, resulting in the wave function being delocalized to bent geometries, the probability of excitation at the photon energies of 6.4 or 6.0 eV (193 or 205 nm) could become more significant. The probability of hot-band excitation as a major contributor in the experimental photodissociation signal has been discussed extensively by Neyer et al.[4] and our results support this conclusion. These speculations will be tested more rigorously in the subsequent dynamical study of the photodissociation process.[38]

3.2. Transition Dipole Moment Surfaces. Figure 7 presents a contour plot of the magnitude of the transition dipole moment surface for the $1\ ^1A'' \leftarrow \tilde{X}\ ^1A'$ transition which is responsible for the first absorption band of the system. This transition dipole moment points in a direction perpendicular to the plane of the N_2O molecule, i.e., along the x-axis. For linear geometries and bond lengths less than 3.65 bohr where the $1\ ^1A''$ state correlates with the $^1\Sigma^-$ state, the transition dipole moment is zero by symmetry.

The transition dipole moment surface for the $2\ ^1A' \leftarrow \tilde{X}\ ^1A'$ transition which is responsible for the second absorption band of the system is shown as a contour plot in Figure 8. This transition moment is a vector field with a y-component and a

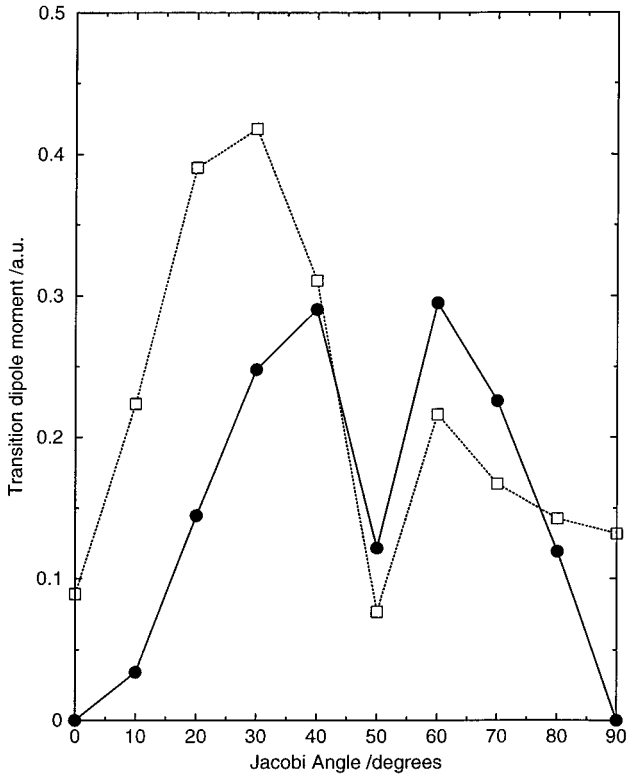

Figure 9. Variation of the *y* (●) and *z* (□) components of the 2 ^{1}A′ ← $\tilde{X}$ ^{1}A′ transition moment, given in au, as a function of Jacobi angle with the N_2−O bond distance set equal to 3.3 bohr. The *z*-axis is along the N−N bond and the *y*-axis is in the molecular plane but perpendicular to the N−N bond (see Figure 1).

z-component which are both located in the plane of the molecule. Therefore, we identify this transition as a "parallel" transition. Only the magnitude of the vector field is illustrated in Figure 8. It is interesting to note that the transition dipole moment surface shows two distinct maxima and the minimum seam between them corresponds directly with the maximum (minimum) energy seam seen on the $\tilde{X}$ ^{1}A′ (2 ^{1}A′) surface. For linear geometries and bond lengths between 3.1 and 3.65 bohr where the 2 ^{1}A′ state should correlate with a state of $^1\Delta$ symmetry, the transition dipole moment should be zero by symmetry. However, since we have performed the calculations using C_s symmetry, there is some symmetry contamination and, while the transition moment is small, it is not identically zero.

The relative contributions of the *y*- and *z*-components to the 2 ^{1}A′ ← $\tilde{X}$ ^{1}A′ transition dipole moment are illustrated in Figure 9 for a fixed R_{N_2-O} bond length of 3.3 bohr. It is readily apparent that both the magnitude of the transition dipole moment and its direction in the *yz*-plane vary as a function of nuclear geometry. While the scalar properties (magnitude) of the dipole moment are important for understanding the form of the absorption spectrum, the vector properties of the transition dipole moments are of utmost importance if one wants to understand the finer details of the photodissociation dynamics.[42,43]

While knowledge of the vector properties is needed for a detailed understanding of the dynamics, a simple comparison of the relative importance of these two transitions can be made by comparing their maximum transition moment amplitudes. The 2 ^{1}A′ ← $\tilde{X}$ ^{1}A′ maximum transition moment of 0.48 is approximately 8 times larger than the 1 ^{1}A″ ← $\tilde{X}$ ^{1}A′ transition moment. Therefore, we expect dissociation via the 2 ^{1}A′ state to be the major contributor to the photodissociation cross section. Note that this simple argument does not take into account Franck−Condon factors but since the 2 ^{1}A′ ← $\tilde{X}$ ^{1}A′ transition moment is globally larger than the 1 ^{1}A″ ← $\tilde{X}$ ^{1}A′ transition moment, the qualitative argument holds. We note that the magnitudes of the transition dipole moment surfaces must still be considered to be somewhat uncertain as it is much more difficult to obtain converged results for this quantity than for the electronic energies of the system.

4. Conclusions

These calculations represent the first systematic treatment of the lowest singlet potential energy surfaces for the N_2O molecule and of the transition dipole moment functions connecting them.

The contour plots clearly show the presence of a conical intersection very close to the Franck−Condon geometry in each of the lowest two electronic excited state potential energy surfaces. These conical intersections will clearly have an important effect on the dissociation dynamics on the surfaces and may be a major factor leading to the high rotational excitation observed in the N_2 photofragments.

The present work has also more clearly revealed another seam of avoided crossing of the two lowest ^{1}A′ symmetry surfaces. There is clear evidence that on further examination this seam of avoided crossing found with the N−N separation held fixed at $r_{N-N} = 2.131\,99$ bohr will reveal a locus of non-symmetry-related conical intersection between these two surfaces. This locus is far removed from the Franck−Condon geometry and is not expected to have any significant effect on the photodissociation dynamics. However, it is likely to be important in N_2 + O collision dynamics.

In a subsequent publication, the potential energy surfaces and the transition dipole moment surfaces will be used to study the photodissociation of N_2O using time-dependent wavepacket techniques. This will hopefully confirm the qualitative arguments presented in this paper by providing a quantitative comparison between theory and experiment.

Acknowledgment. A.B. thanks the Natural Sciences and Engineering Research Council of Canada for the award of a post-doctoral fellowship. P.J. thanks PPARC for financial support. We thank the EPSRC for the provision of a computer under grant number GR/M34799. We also thank Dr. C. Wilson for technical assistance.

Supporting Information Available: The ab initio energies are available for the $\tilde{X}$ ^{1}A′, 2 ^{1}A′, and 1 ^{1}A″ electronic states (Tables S.1, S.2, and S.3). The ab initio electronic transition dipole moments for the 1 ^{1}A″ ← $\tilde{X}$ ^{1}A′ (Table S.4) and 2 ^{1}A′ ← X ^{1}A′ (Table S.5) transitions are also provided. This material is available free of charge via the Internet as http://pubs.acs.org.

References and Notes

(1) Brouard, M.; Duxon, S. P.; Enriquez, P. A.; Simons, J. P. *J. Chem. Phys.* **1992**, *97*, 7414.

(2) Brouard, M.; Lambert, H. M.; Short, J.; Simons, J. P. *J. Phys. Chem.* **1995**, *99*, 13571.

(3) Alexander, A. J.; Aoiz, F. J.; Brouard, M.; Burak, I.; Fujimura, Y.; Short, J.; Simons, J. P. *Chem. Phys. Lett.* **1995**, *262*, 589.

(4) Neyer, D. W.; Heck, A. J. R.; Chandler, D. W. *J. Chem. Phys.* **1999**, *110*, 3411.

(5) Teule, J. M. Ph.D. Thesis, Vrije Universiteit, 1997.

(6) Suzuki, T.; Katayanagi, H.; Mo, Y.; Tonokura, K. *Chem. Phys. Lett.* **1996**, *256*, 90.

(7) Hanisco, T. F.; Kummel, A. C. *J. Phys. Chem.* **1993**, *97*, 7242.

(8) Springsteen, L. L.; Satyapal, S.; Matsumi, Y.; Dobeck, L. M.; Houston, P. L. *J. Phys. Chem.* **1993**, *97*, 7239.

(9) Felder, P.; Haas, B.-M.; Huber, J. R. *Chem. Phys. Lett.* **1991**, *186*, 177.
(10) Shafer, N.; Tonokura, K.; Matsumi, Y.; Tasaki, S.; Kawasaki, M. *J. Chem. Phys.* **1991**, *95*, 6218.
(11) Selwyn, G. S.; Johnston, H. S. *J. Chem. Phys.* **1981**, *74*, 3791.
(12) Hopper, D. G. *J. Chem. Phys.* **1984**, *80*, 4290.
(13) Nakamura, H.; Kato, S. *Chem. Phys. Lett.* **1998**, *297*, 187.
(14) Wong, A. T.; Bacskay, G. B. *Chem. Phys. Lett.* **1993**, *207*, 360.
(15) Frind, C.; Asbrink, L.; Lindholm, F. *Chem. Phys.* **1978**, *27*, 169.
(16) Winter, N. W. *Chem. Phys. Lett.* **1975**, *33*, 300.
(17) Chutjian, A.; Segal, G. A. *J. Chem. Phys.* **1972**, *57*, 3069.
(18) Peyerimhoff, S. D.; Buenker, R. J. *J. Chem. Phys.* **1968**, *49*, 2473.
(19) McLean, A. D.; Yoshimine, M. *J. Chem. Phys.* **1966**, *45*, 3676.
(20) Nakamura, H.; Kato, S. *J. Chem. Phys.* **1999**, *110*, 9937.
(21) Chang, A. H.; Yarkony, D. R. *J. Chem. Phys.* **1993**, *99*, 6824.
(22) MOLPRO is a package of ab initio programs written by Werner, H.-J.; Knowles, P. J., with contributions from Almlöf, J.; Amos, R. D.; Berning, A.; Deegan, M. J. O.; Eckert, F.; Elbert, S. T.; Hampel, C.; Lindh, R.; Meyer, W.; Nicklass, A.; Peterson, K.; Pitzer, R.; Stone, A. J.; Taylor, P. R.; Mura, M. E.; Pulay, P.; Schuetz, M.; Stoll, H.; Thorsteinsson, T.; Cooper., D. L.
(23) Werner, H.-J.; Knowles, P. J. *J. Chem. Phys.* **1985**, *82*, 5053.
(24) Knowles, P. J.; Werner, H.-J. *Chem. Phys. Lett.* **1985**, *115*, 259.
(25) Werner, H.-J.; Knowles, P. J. *J. Chem. Phys.* **1988**, *89*, 5803.
(26) Knowles, P. J.; Werner, H.-J. *Chem. Phys. Lett.* **1988**, *145*, 514.
(27) Ho, T.-S.; Rabitz, H. *J. Chem. Phys.* **1996**, *104*, 2584, and references therein.
(28) Jimeno, P.; Gray, M. D.; Balint-Kurti, G. G. *J. Chem. Phys.* **1999**, *111*, 4966.
(29) Dunning, T. H., Jr. *J. Chem. Phys.* **1990**, *90*, 1007.
(30) Kendall, R. A.; Dunning, T. H., Jr.; Harrison, R. J. *J. Chem. Phys.* **1992**, *96*, 6769.
(31) Dunning, T. H. *J. Chem. Phys.* **1970**, *53*, 2823.
(32) Woywood, C.; Stengle, M.; Domcke, W.; Flöthmann, H.; Schinke, R. *J. Chem. Phys.* **1997**, *107*, 7282.
(33) Domcke, W.; Woywood, C. *Chem. Phys. Lett.* **1993**, *216*, 362.
(34) Braunstein, M.; Hay, P. J.; Martin, R. L.; Pack, R. T. *J. Chem. Phys.* **1991**, *95*, 8239.
(35) Xantheas, S. S.; Atchity, G. J.; Gilbert, S. T.; Ruedenberg, K. *J. Chem. Phys.* **1991**, *94*, 8054.
(36) Borowski, P.; Fülscher, M.; Malmqvist, P. Å.; Roos, B. O. *Chem. Phys. Lett.* **1991**, *237*, 195.
(37) Suzuki, T.; Katayanagi, H.; Nanbu, S.; Aoyagi, M. *J. Chem. Phys.* **1998**, *109*, 5778.
(38) Brown, A.; Balint-Kurti, G. G. Unpublished work.
(39) Langhoff, S. R.; Davidson, E. R. *Int. J. Quant. Chem.* **1974**, *8*, 61. Silver, D. W.; Davidson, E. R. *Chem. Phys. Lett.* **1978**, *52*, 403.
(40) Okabe, H. *Photochemistry of Small Molecules*; John Wiley and Sons: New York, 1978; Chapter 6.
(41) Chase, M. W., Jr.; Davies, C. A.; Downey, J. R., Jr.; Frurip, D. J.; McDonald, R. A.; Syverud, A. N. *JANAF Thermochemical Tables*, 3rd ed; American Chemical Society: Washington, DC, 1986.
(42) Offer, A. R.; Balint-Kurti, G. G. *J. Chem. Phys.* **1994**, *101*, 10416.
(43) Offer, A. R.; Balint-Kurti, G. G. *J. Chem. Phys.* **1996**, *104*, 563.